Chemistry Europe
European Chemical Societies Publishing

A Photo- and Redox-Driven Two-Directional Terthiazole-Based Switch: A Combined Experimental and Computational Investigation

Nicolò Baggi,[a] Anne Léaustic,*[a] Sihem Groni,[b] Elodie Anxolabéhère-Mallart,[b] Régis Guillot,[a] Rémi Métivier,[c] François Maurel,*[d] and Pei Yu*[a]

Abstract: Terthiazoles with redox-active substituents like an N-methyl pyridinium group and ferrocene have been synthesized and their photo- and electro-chromic behaviors were investigated. The presence of two lateral N-methyl pyridinium substituents in the structure of terthiazole proved to be effective in inducing not only the reductive ring-closure of the terthiazole core but also its oxidative ring-opening reaction, leading to the first terarylene-based switch able to fully operate both photochemically and electrochemically. Moreover, the large increase in the redox potential between its open and closed form (700 mV) means that a part of the photon energy necessary to trigger the cyclization is stored in the form of chemical potential available for other works. Introduction of a second redox-active unit such as ferrocene onto the central thiazolyl moiety is found to inhibit the photochromism of the switch but not its redox switchability, which, instead, got improved for the ring-opening reaction via the redox properties of the ferrocenyl unit. The optical and redox properties of the switch in its different oxidation states are analyzed with the aid of DFT calculations in order to rationalize different switching processes.

Introduction

Photochromic molecules have been extensively investigated as molecular switches for the design of various photo-responsive systems for a broad range of potential applications.[1] One popular family of such molecular photoswitches are diarylethenes as they can be reversibly switched with low fatigue between two thermally stable isomers, a less conjugated open form and a more conjugated closed form.[2] Another interesting feature that makes diarylethenes even more appealing as molecular switches is the possibility of driving the isomerization by an electrochemical stimulus in addition to light.

To date, most studies have focused on the electron-rich dithienylethenes and their oxidation induced ring-closing or ring-opening reaction depending on their substitution patterns.[3–11] In comparison, examples of reductive electrocyclization are rare and generally require the presence of strong electron withdrawing groups such as N-methylpyridinium connected to the photochromic dithienylethene or dithiazolylethene core.[12–14] However, recent works showed that dithienylethenes with appropriate cyano-substitution or an extended π system could also lead to reductive ring-closure, albeit with much more negative potentials.[11] It is worth noting that in most cases the redox input triggers only one-way isomerization and cannot be used to bring the diarylethene back to its initial state. There are only few reports on bidirectional photo- and redox-switchable diarylethenes.[9,10,13,15]

Terarylenes are a sub-class of diarylethenes with good photochromic properties.[16–19] Compared to diarylethenes with classical central ethene moieties such as perfluorocyclopentene, cyclopentene and maleimide etc.,[2] the central aryl group offers an extra site available for further functionalization of the switch in addition to the two lateral aryl groups.[20–22] For instance, we have shown that a properly designed terthiazolylene could act as photochromic ligand and give rise to metal complexes with interesting photo-responsive properties.[23] With regard to redox-responsive behavior, different terarylenes (aryl = thiazolyl, thienyl group or a combination of the two) have been reported to undergo oxidation induced ring-opening of their respective closed forms and, moreover, this ring-opening reaction was found to proceed via an auto-catalytic chain reaction mechanism with an efficiency well above 100%,[24,25] but no reductive cyclization is known for terarylenes, to our knowledge. To investigate the possibility of combining both the oxidative ring-opening and the reductive ring-closing reaction within terar-

[a] N. Baggi, Dr. A. Léaustic, Dr. R. Guillot, Dr. P. Yu
Université Paris-Saclay, CNRS, Institut de Chimie Moléculaire et des Matériaux d'Orsay
91405, Orsay (France)
E-mail: anne.leaustic@universite-paris-saclay.fr
pei.yu@universite-paris-saclay.fr

[b] Dr. S. Groni, Dr. E. Anxolabéhère-Mallart
Université de Paris, Laboratoire d'Electrochimie Moléculaire, CNRS, 75013, Paris (France)

[c] Dr. R. Métivier
Université Paris-Saclay, ENS Paris-Saclay, CNRS, PPSM
91190 Gif-sur-Yvette (France)

[d] Prof. F. Maurel
Université de Paris, ITODYS, CNRS
75006, Paris (France)
E-mail: maurel@u-paris.fr

Supporting information for this article is available on the WWW under https://doi.org/10.1002/chem.202101945

ylenes, we set up to design appropriately N-methylpyridinium-substituted terarylenes, since this functionalization is the most effective for triggering reductive cyclization of diarylethenes at accessible potentials,[12,14] and also to study how the properties of such a bi-directional photo- and redox-switch, if confirmed, could possibly be modulated by tuning the structure of the central aryl group. To this end, two dicationic terthiazole-based molecules are synthesized and fully characterized (Scheme 1).

Thiazoles are chosen as aromatic groups to build terarylenes because of their easy synthetic access and also the generally good photochromic properties of corresponding dithiazolylethenes[26–28] and terthiazolylethenes.[29,30] While the ferrocene substituent on the central phenylthiazole group may provide a convenient way to tune the photo- and electrochromic properties of the switch as its electronic nature can be reversibly switched between a diamagnetic electron donor (Fc) and a paramagnetic electron acceptor (Fc^+) via its redox chemistry. Such a redox switch has proven efficient for the thermal ring-opening of dithienylethenes[8] and effective to unlock the photochromic reactivity, giving rise to interesting redox-gated photochromism.[31]

Combined photochemical, electrochemical and spectro-electrochemical studies show that (1) introduction of two lateral N-methylpyridinium groups does trigger the expected reductive ring-closing reaction in terthiazole-based switches ($\mathbf{2o}^{2+}$ and $\mathbf{4o}^{2+}$) while maintaining their ring-opening ability of their respective closed form ($\mathbf{2c}^{2+}$ and $\mathbf{4c}^{2+}$); (2) the presence of the ferrocenyl substituent on the central phenylthiazole moiety has a drastic impact on the photochromic reactivity of the dicationic terthiazole $\mathbf{4o}^{2+}$ as well as its neutral precursor **3o**, but doesn't significantly alter its redox-driven bidirectional switchability. Finally, theoretical calculations based on DFT are performed in order to understand and rationalize the way the photochromic and electrochromic properties are impacted by the oxidation state of the switch.

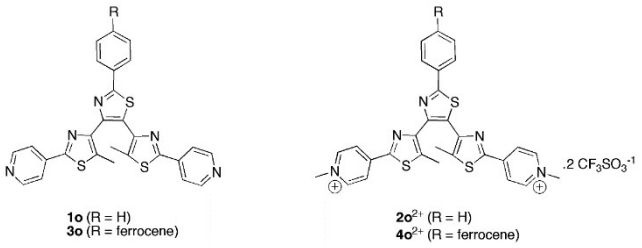

Scheme 1. The four investigated terthiazole-based switches.

Results and Discussion

Syntheses and characterizations

The two neutral terthiazole-based switches **1o** and **3o** can be readily prepared with high yields by a double Suzuki coupling between 2-(4-pyridyl)-4-(4,4,5,5-tetramethyl-1,3,2-dioxoborolan-2-yl)-5-methyl-thiazole and 2-phenyl-4,5-di-bromo-thiazole or 2-(4-ferrocenyl-phenyl)-4,5-di-bromo-thiazole, respectively, as shown in Scheme 2. Note that the latter can be readily prepared by a one-pot reaction (Scheme 2).

The bis-N-methylation is achieved using an excess of iodomethane before the iodide is exchanged with silver triflate (AgOTf) to afford $\mathbf{2o}^{2+}$ or $\mathbf{4o}^{2+}$, respectively, with two triflates as counter anions. The four terthiazoles are fully characterized by standard analytic techniques. In the case of $\mathbf{2o}^{2+}$, single-crystal analyses also confirm the expected structure, as shown in Figure 1 (more details can be found in the Supporting Information).

Photochromic properties

The photochromic behaviors of the neutral and dicationic terthiazoles have been investigated in acetonitrile at room temperature by using steady-state absorption spectroscopy and their main photochromic data are listed in Table 1.

As shown in Figure 2 both the neutral terthiazole **1o** and the dicationic one $\mathbf{2o}^{2+}$ are photochromic in solution and can be cleanly photo-switched between their respective open (**1o** and $\mathbf{2o}^{2+}$) and closed forms (**1c** and $\mathbf{2c}^{2+}$) with high conversion ratio (Table 1).

However, the N-methylation of the two pyridines results in important changes in the main photochromic properties (Table 1). Firstly, the main absorption bands of the dicationic terthiazole $\mathbf{2}^{2+}$ in both its open and closed forms are

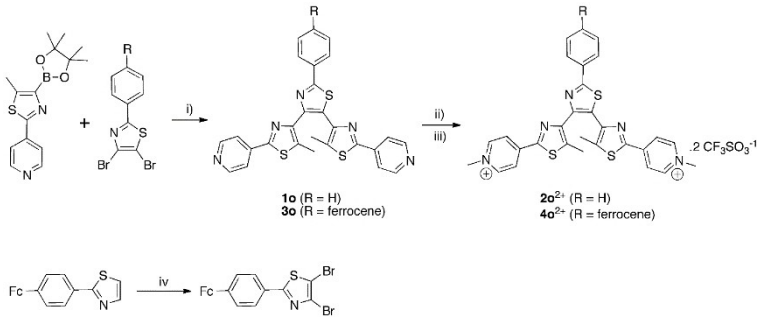

Scheme 2. Synthetic route of the four terthiazole-based switches. (i) $Pd(Ph_3)_4$ cat. CsF-dioxane/reflux; (ii) MeI (excess)-CH_2Cl_2/reflux; (iii) AgOTf; (iv) LDA-THF followed by $C_2Br_2Cl_4$.

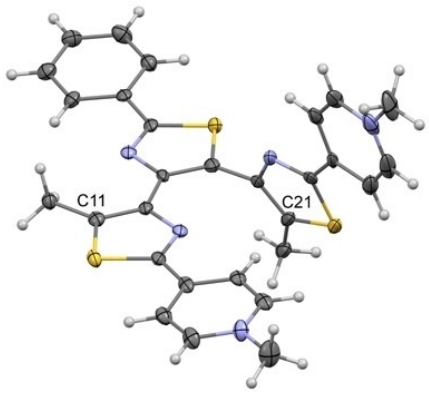

Figure 1. An ORTEP drawing of $\mathbf{2o}^{2+}$. Thermal ellipsoids are shown at the 30% level. Anions and solvent molecules are omitted for clarity. Deposition Number 2084834 contains the supplementary crystallographic data for this paper. These data are provided free of charge by the joint Cambridge Crystallographic Data Centre and Fachinformationszentrum Karlsruhe Access Structures service.

significantly redshifted as compared to those of the neutral precursor terthiazole **1** (Table 1). Secondly, the quantum yield of the cyclization is more than halved while that of the cycloreversion is decreased by ca. seven-fold in comparison to those of the neutral terthiazole precursor (Table 1). Similar effects on quantum yield upon N-methylation of pyridine were reported for dithiazolylethenes.[14] Thirdly, the closed form of the neutral terthiazole (**1c**) is thermally stable at room temperature while the closed form of the dicationic one ($\mathbf{2c}^{2+}$) slowly reverts back to its open form ($\mathbf{2o}^{2+}$). The smaller thermal stability of the closed form is not unexpected as the newly formed C–C single bond is weakened by the two strongly electron-withdrawing N-methyl pyridinium groups. By monitoring this thermal decay at different temperatures, an activation energy (E_a) of 94 kJmol^{-1} for this back reaction is found, with an estimated half-lifetime ($\tau_{1/2}$) of ca. 2 h at room temperature and around 6 h at 15 °C. Finally, unlike **1o**, $\mathbf{2o}^{2+}$ is weakly fluorescent, with an emission maximum around 630 nm and a quantum yield of ca. 1.2% (Figure S1). Since $\mathbf{2c}^{2+}$ is not fluorescent an on-off switching of this fluorescence is observed when $\mathbf{2o}^{2+}$ photo-isomerizes to $\mathbf{2c}^{2+}$.

In the solid state, **1o** and $\mathbf{2o}^{2+}$ do not show any detectable photochromic activity. In the case of $\mathbf{2o}^{2+}$, it is hard to tell whether the two methyl groups are in the photo-reactive antiparallel or the photo-inactive parallel mode as they are sited in two almost perpendicular plans, while the distance separating the two photo-reactive carbon atoms (C11 and C21) is 5.32 Å (Figure 1), which is anyhow well above the admitted upper limit (4.2 Å) for the observation of crystalline state photochromism.[32]

The neutral ferrocene-substituted terthiazole **3o** is orange in solution as its absorption in the visible is mainly dominated by the ferrocenyl moiety (Figure S2). Upon UV irradiation (365 nm) no detectable spectral changes could be observed. The photochromic reactivity of the core **1o** is thus completely inhibited by the introduction of ferrocene. However, a very small yet detectable spectral change could be seen after the oxidation of the ferrocenyl moiety to ferrocenium using Cu(OTf)$_2$ (Figure S2).

$\mathbf{4o}^{2+}$ is very slightly photochromic in solution, and upon oxidation of ferrocenyl to ferrocenium an enhancement of photochromic reactivity could be observed (Figure S3), even though it is far below what has been reported for the redox-gated photochromism.[31] The reasons for the inhibition and the very partial recovery of the photochromic reactivity via oxidation of the ferrocene moiety are not clearly understood yet, but it is reasonable to think that the introduction of electron-rich ferrocene into these rather electron-poor terthiazoles would confer a certain degree of charge-transfer (CT) character to the otherwise ferrocene-centered absorption bands between 400 and 550 nm (Figure S2 and 3). Since CT bands are often associated to a lower cyclization efficiency in diarylethenes,[33–35] one would expect some enhancement of photochromic reactivity upon oxidation of ferrocene to ferrocenium.

Electrochemical properties

The electrochemical properties of the four terthiazoles have been investigated using cyclic voltammetry (CV) at room temperature in acetonitrile and the main data reported in Table 2.

1o is not redox active over a large range of the potential window of the electrolytic solution while its closed form **1c** is characterized by one irreversible oxidation at ca. 0.90 V and two almost reversible reduction waves at −0.88 and −1.22 V,

Table 1. Main photochromic data of the four terthiazole-based switches.

	λ_{max} [nm]/ε [M^{-1}cm^{-1}]	$\phi_{o\text{-}c}$	Conversion ratio [λ_{irr}/nm]		λ_{max} [nm]/ε [M^{-1}cm^{-1}]	$\phi_{c\text{-}o}$
1o	272/26990 319/30360	0.36	94% (320)	**1c**	264/28000 308/19465 373/18690 632/13540	0.015
$\mathbf{2o}^{2+}$	257/20180 322/28900 375/17290	0.15	95% (365)	$\mathbf{2c}^{2+}$	277/32780 420/10370 744/17430	0.002
3o	455/3540 329/60635 294/49310			**3c**		
$\mathbf{4o}^{2+}$	340/42775			$\mathbf{4c}^{2+}$		

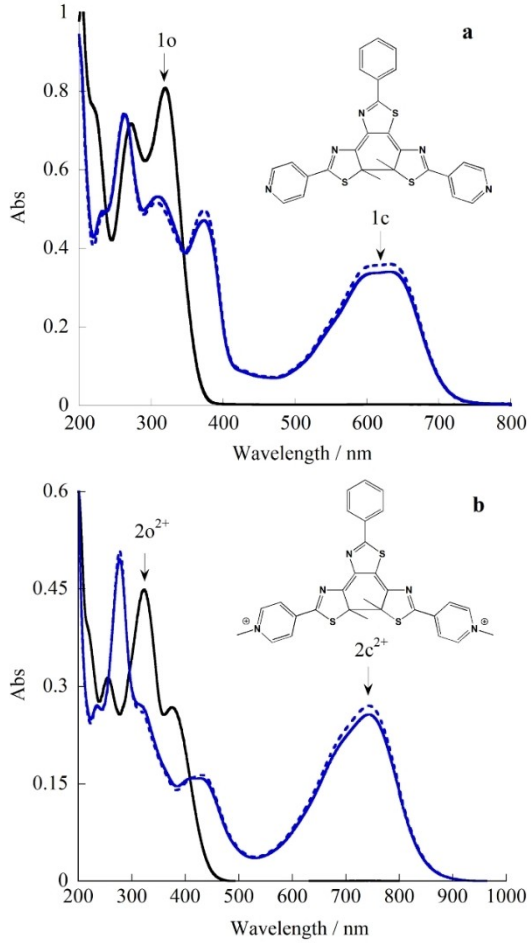

Figure 2. Absorption spectra of **1o** (2.66 10^{-5} M in 1 cm cell) (a) and **2o**$^{2+}$ (1.55 10^{-4} M in 1 mm cell) (b) in MeCN at RT along with their photostationary state (PSS, solid blue line) at 320 and 365 nm, respectively, and the calculated spectra of their respective closed form (dotted blue line).

Table 2. Redox potentials E (vs. SCE) of the four terthiazole-based switches measured in 0.1 M of Bu_4NPF_6 acetonitrile solution at RT.

	$E_{1/2}$ or E_p	ΔE [mV]		$E_{1/2}$ or E_p	ΔE [mV]
1o	1.5 (irr)		**1c**	0.90 (irr), 1.5 (irr)	
				−0.88	70
				−1.22 (qr)	100
2o^{2+}	−0.91 (qr)		**2c**$^{2+}$	1.10 (irr)	
				−0.21	52
3o	1.60 (irr)		**3c**		
	0.48[a]	60			
4o^{2+}	1.6 (irr)		**4c**$^{2+}$	1.22 (irr)	
	0.46	90		0.46	90
	−0.90 (qr)	110		−0.21	56

[a] Solvents: 20% dichloromethane in acetonitrile.

respectively (Figure S4). Unlike the oxidative ring-opening reaction reported for some terarylenes,[24,25] the irreversible oxidation of **1c** does not result in the formation of **1o**.

As expected, **2o**$^{2+}$ is not electroactive toward oxidation because the strong electron-withdrawing N-methyl pyridinium groups make it harder to oxidize than **1o**. Meanwhile, its reduction is quasi reversible with $E_{1/2} = -0.91$ V, as shown in Figure 3a. On the back scan one anodic peak is observed at a much less negative potential, with $E_{1/2} = -0.21$ V, and its intensity grows at the expense of the initial one in subsequent CVs. This new redox-active species is unambiguously assigned to the closed form **2c**$^{2+}$ as the CV of the same solution upon UV irradiation is characterized by the two same redox waves, with the relative intensity of the new one increasing with UV irradiation time at the expense of that of **2o**$^{2+}$. In other words, **2o**$^{2+}$ does show the expected ring-closing reaction to give **2c**$^{2+}$ after re-oxidation at potential higher than −0.21 V. Note also that this ring-closing reaction is rather slow as its characteristic wave at −0.21 V gradually decreases in intensity with increasing scan rate and, eventually, completely disappears with a scan rate between 3–4 V s^{-1}, which puts the rate of the ring-closing reaction in the range of ~10 s^{-1} (Figure S5a).

In addition to this reversible peak at −0.21 V, **2c**$^{2+}$ is also characterized by an irreversible peak at 1.10 V of lower intensity when the first anodic back scan is swept to 1.40 V, as shown in Figure 3b. It is important to note that, unlike the CV run

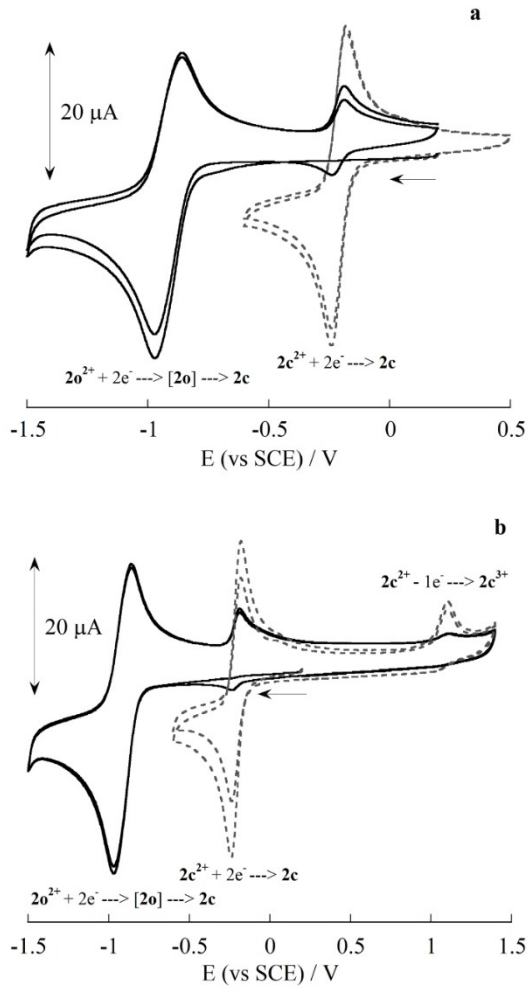

Figure 3. Cyclic voltammograms of **2o**$^{2+}$ (plain plots) (1.0 mM) in MeCN containing 0.10 M Bu_4NPF_6 at 20 °C, v = 0.1 V s^{-1} and those of its UV irradiated solution (dotted plots): a) reductive cyclization; b) reductive cyclization and oxidative ring-opening.

between 0.2 V and −1.5 V (Figure 3a), the cathodic scan of the second consecutive CV sees a decrease of the intensity of the peak at −0.21 V and a concomitant increase of that at −0.91 V. In other words, the oxidation at 1.10 V speeds up considerably the pre-existing thermal ring-opening reaction of $\mathbf{2c}^{2+}$, which is not visible otherwise on the time scale of cyclic voltammetry at room temperature as shown in Figure 3a (left part), where an accumulation of $\mathbf{2c}^{2+}$ is instead observed in the second consecutive cyclic voltammogram. The lower intensity of this irreversible oxidation peak at 1.10 V is likely ascribed to a similar electro-catalytic oxidation process operating in the diffusion layer previously reported for bis N-methyl pyridinium substituted dithienylhexafluorocyclopentenes at, however, a significantly higher potential (ca. 1.5 V vs. SCE).[13] Briefly, as soon as $\mathbf{2c}^{2+}$ is oxidized, the unstable $\mathbf{2c}^{3+}$ ring-opens to $\mathbf{2o}^{3+}$ which, being a stronger oxidizer than $\mathbf{2}^{2+}$, would in turn immediately oxidize a neighboring molecule of $\mathbf{2c}^{2+}$ to $\mathbf{2c}^{3+}$. Such a chain reaction would lead to a local depletion of $\mathbf{2c}^{2+}$ in the diffusion layer before any significant change in the current can be recorded. However, as for the reductive ring-closing reaction, this oxidative ring-opening process is not very fast neither because the irreversible peak at 1.1 V observed at low scan rate tends to become more reversible at higher scan rates and, at 4 $V s^{-1}$, the limit of our standard equipment, this tendency can clearly be discerned (Figure S5b), suggesting a faster ring-opening reaction than the ring-closing one.

3o is not electroactive toward reduction down to −1.5 V and presents an expected ferrocene-centered reversible oxidation at 0.48 V followed by an irreversible oxidation that breaks down the molecule (Figure S6).

In comparison, the cyclic voltammograms of $\mathbf{4o}^{2+}$ are more interesting (Figure 4).

Qualitatively, the cyclic voltammograms of $\mathbf{4o}^{2+}$ are quite similar to those of $\mathbf{2o}^{2+}$ except for the presence of the redox couple associated to the ferrocenyl moiety. It is therefore reasonable to think that $\mathbf{4o}^{2+}$ also undergoes similar reductive ring closure to give the corresponding ring-closed form $\mathbf{4c}^{2+}$ after re-oxidation at the same potential (Table 2). However, the ferrocenyl substituent brings about some notable advantages. (1) As a built-in one-electron reference it allows to conclude with confidence that the reduction of $\mathbf{4o}^{2+}$ at −0.91 V involves two electrons and, by extension also its re-oxidation at −0.21 V to give $\mathbf{4c}^{2+}$ (Figure 4a). By analogy, the same conclusion can be drawn for $\mathbf{2o}^{2+}$ discussed above. (2) Unlike **2c**, Figure 4b shows that the first oxidation of $\mathbf{4c}^{2+}$ is localized at the ferrocenyl site as expected and the second one, irreversible and weak in intensity, occurs at higher potential than for $\mathbf{2o}^{2+}$ (1.22 vs. 1.10 V, Figure 4b), likely due to the electron-withdrawing nature of ferrocenium. (3) More importantly, the ring-opening of $\mathbf{4c}^{2+}$ can already be seen with the oxidation of ferrocene to ferrocenium at a much lower potential than for $\mathbf{2c}^{2+}$ (Figure 4b). However, note that ring-opening here would not proceed in the same way as the one observed for $\mathbf{2o}^{2+}$ because the oxidation potential of the ferrocenyl moiety is the same for both $\mathbf{4o}^{2+}$ et $\mathbf{4c}^{2+}$, so no electro-catalytic chain reaction as that for $\mathbf{2c}^{2+}$ is expected. The oxidation of the electron donating ferrocene to the electron-withdrawing ferrocenium would just accelerate the pre-existing thermal ring-opening reaction of $\mathbf{4c}^{2+}$.

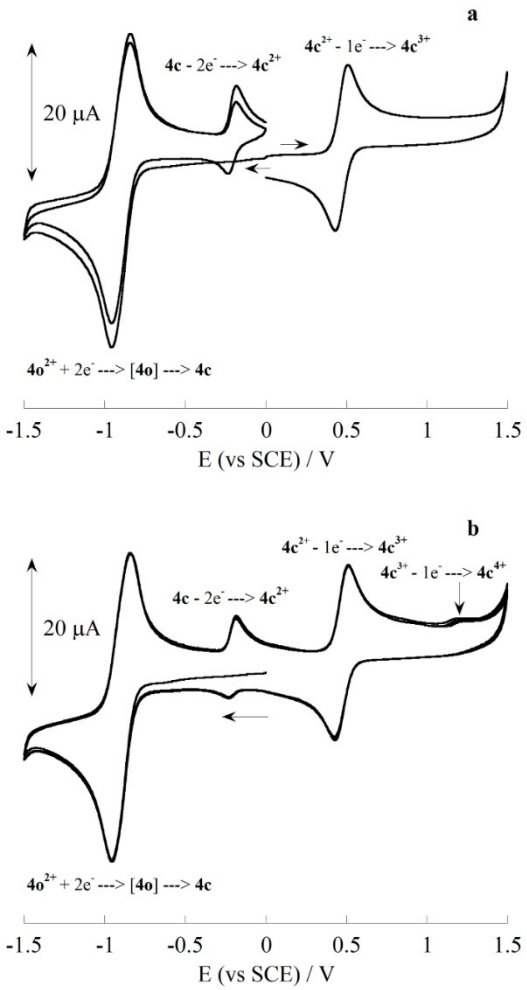

Figure 4. Cyclic voltammograms of $\mathbf{4o}^{2+}$ (1.0 mM) in MeCN containing 0.10 M Bu_4NPF_6 at 20 °C, v = 0.1 Vs^{-1}: a) reductive cyclization and reversible oxidation of the ferrocenyl moiety; b) reductive cyclization and oxidative ring-opening.

Spectroelectrochemical studies

Although it is clear from the data of cyclic voltammetry that the reductive cyclization in $\mathbf{2o}^{2+}$ and $\mathbf{4o}^{2+}$ involves two electrons, two pathways are still possible. The cyclization may occur either at one-electron reduction stage as reported for related dithienylethene[12] or after a two-electron reduction as described for a similarly substituted dithiazolylethene.[14] To answer the question, low temperature spectroelectrochemical experiment is performed in the case of $\mathbf{2o}^{2+}$ as it can provide the spectroscopic characteristics of the transient species involved, necessary for the identification of the reaction pathway.

The electrolysis of $\mathbf{2o}^{2+}$ is conducted at −25 °C under different fixed potentials and monitored in situ by absorption spectroscopy, as shown Figure 5.

When reduced at −1.10 V the spectrum changes from that of $\mathbf{2o}^{2+}$ with its characteristic bands in the UV region to a new one with two absorption bands in the visible region at the end of the electrolysis (Figure 5a), corresponding likely to the twice reduced closed form **2c** (see below). Subsequent electrolysis at 0.0 V eventually leads to an absorption spectrum (Figure 5b) very close to that of photo-chemically generated $\mathbf{2c}^{2+}$, confirming the expected reductive ring-closure of $\mathbf{2o}^{2+}$. In addition, the conversion is found to be more than 90%.

Now let's have a closer look at the spectral evolution during the course of the electrolysis at −1.10 V (Figure 5a). The decrease in intensity of the characteristic bands of $\mathbf{2o}^{2+}$ in the UV region (257, 322 and 375 nm) is accompanied by the appearance of a new one at 420 nm, which gains first in intensity before fading away in favor of two new bands in the visible (535 and 725 nm). As it will be seen later, the absorption band at 420 nm is assigned to the twice reduced open form **2o**, indicating thereby that the ring-closure is taking place when $\mathbf{2o}^{2+}$ is two-electron reduced.

A similar experiment but with the second electrolysis directly conducted at 1.40 V is carried out and the absorption spectral evolution given in Figure 6.

Instead of the electrolysis sequence used in Figure 5 that leads to the closed form $\mathbf{2c}^{2+}$, an electrolysis at 1.40 V following that at −1.10 V produces an absorption spectrum almost identical to that of the initial open form $\mathbf{2o}^{2+}$, confirming the oxidative ring-opening reaction and also the cleanliness of the two redox induced reactions because more than 90% of $\mathbf{2o}^{2+}$ is recovered after a complete redox driven cycle.

Based on these experimental data, Scheme 3 summarizes the proposed redox processes involved in the reductive ring-closure and the oxidative ring-opening reaction of $\mathbf{2o}^{2+}$.

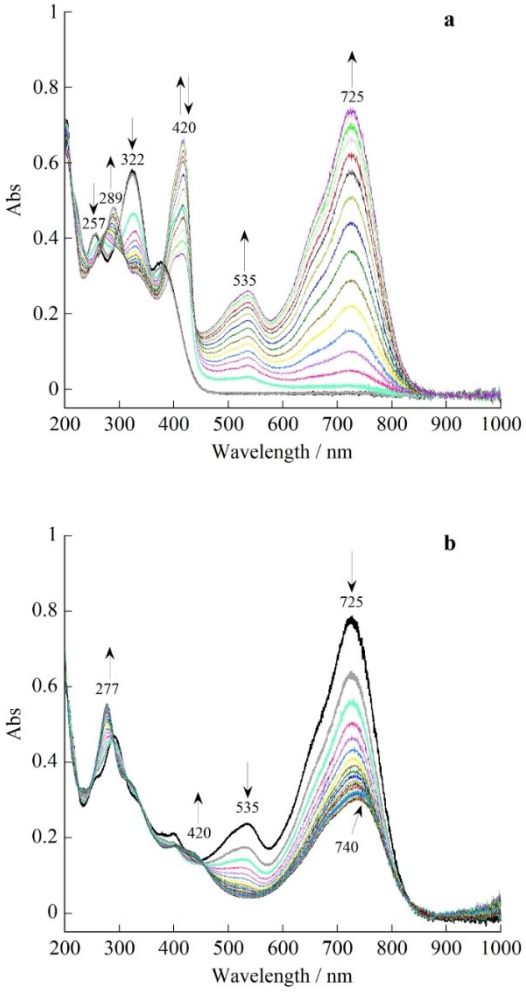

Figure 5. Absorption spectral changes of $\mathbf{2o}^{2+}$ (1.75 10^{-4} M) during electrolysis (a) at −1.10 V and then (b) at 0.0 V (vs. SCE) in 0.2 M Bu_4NPF_6/MeCN at −25 °C.

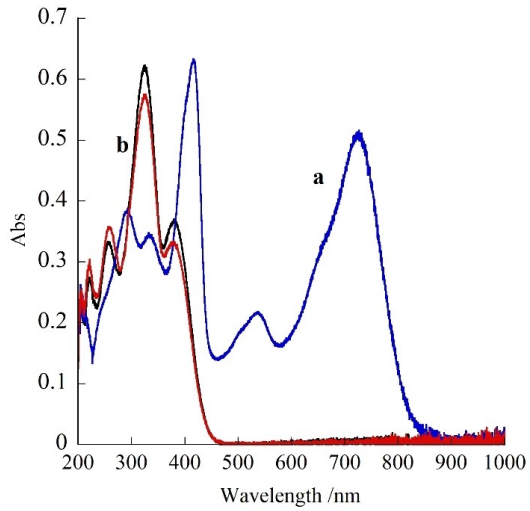

Figure 6. Absorption spectra of $\mathbf{2o}^{2+}$ (1.75 10^{-4} M) (black) after electrolysis (a) at −1.10 V (blue) and then (b) at 1.40 V (red) (vs. SCE) in 0.2 M Bu_4NPF_6/MeCN at −25 °C.

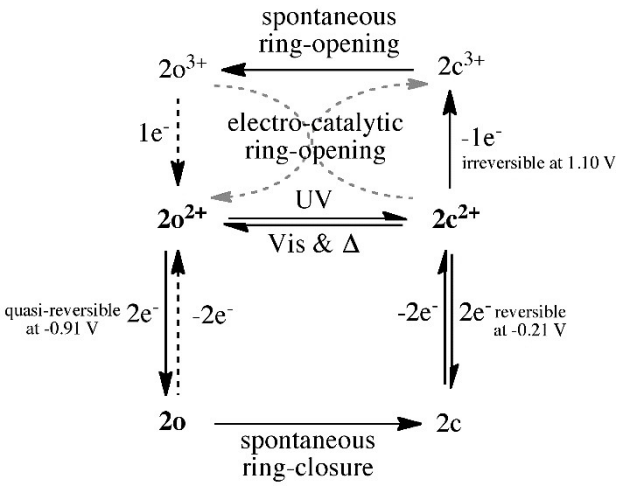

Scheme 3. Photochemical and electrochemical transformation between $\mathbf{2o}^{2+}$ and $\mathbf{2c}^{2+}$.

Theoretical calculations

In order to better understand and rationalize the bidirectional photo- and electro-chemical switching behaviors, we have investigated in detail the switch **2** using DFT and TD-DFT calculations.

Geometrical calculations on $\mathbf{2o}^{2+}$ show three possible conformations (one antiparallel and two parallel) close in energy. According to the Woodward-Hoffman rules the intramolecular cyclization of $\mathbf{2o}^{2+}$ involving 6-π electron is photochemically allowed during conrotatory motion of the two lateral thiazolyl groups. It means that only the antiparallel conformation is a photo-active conformer and we will discuss here only the results for the open and the closed form under different oxidation states starting with the antiparallel open form conformation at the ground state.

Ground state reactivity: ring-closure reaction

We calculated the potential energy surface for the cyclization reaction at the ground state. Table 3 reports the relative energies of the closed form and of the transition states for the cyclization at the ground state as well as the distance between reactive carbon in the transition state. Pathways for the different redox states are summarized in Figure 7.

The ground state energy difference between open and closed isomers controls the thermal stability. The cyclization reaction has to overcome an energy barrier which, according to calculations, correlates with the ground state energy difference. This correlation can be explained with the Polanyi rule.[36] When the reaction becomes exothermic, the energy barrier for cyclization is small. The energy barrier becomes greater when the reaction is endothermic. For instance, the energy barrier is very high for the dicationic state $\mathbf{2o}^{2+}$ (190.1 kJmol^{-1}) and the distance between the two reactive carbon atoms is relatively short (1.728 Å), explaining the late transition state in agreement with the high-energy barrier and the endothermic character of the reaction (74.9 kJmol^{-1}). The ring-closure energy profile strongly changes upon redox reaction and becomes less endothermic by one-electron oxidation or reduction and even exothermic upon two electron reduction while the energy barrier is lowered and the transition state is reached with a longer C–C distance. A nice correlation between the ring-closing activation energy and the energy of the reaction is shown in Figure 8.

As expected the dicationic open form $\mathbf{2o}^{2+}$ is more stable than its closed form $\mathbf{2c}^{2+}$. When it is reduced, the opposite becomes true, particularly in the case of the two-electron reduction where the closed form **2c** is strongly stabilized by as much as 120.8 kJmol^{-1}. This is in agreement with the spontaneous ring-closure observed when $\mathbf{2o}^{2+}$ is reduced twice.

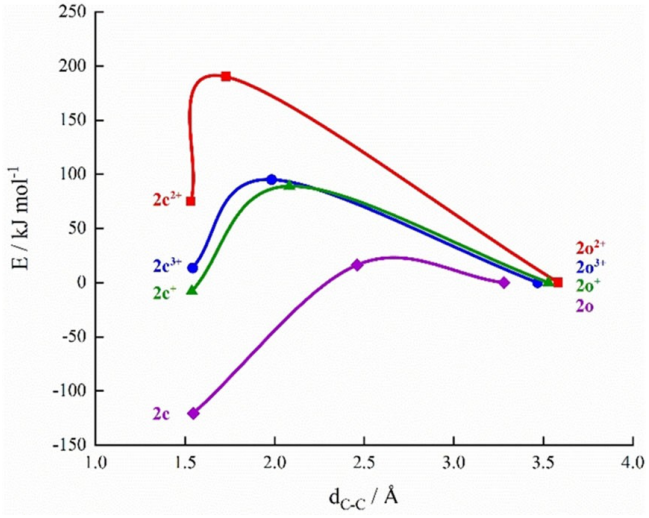

Figure 7. Reaction pathway for the ring-closure at ground state for different redox state of the switch **2**.

Table 3. Relative energies of the closed form and the transition state for the cyclization at the ground state of the switch **2** as well as the distance between the two reactive carbon atoms in the transition state.

Redox state	E [kJ/mol]	$d_{C\text{-}C}$ [Å]
+3		
$\mathbf{2o}^{3+}$ (antipar)	0	3.487
TS	95.2	1.982
$\mathbf{2c}^{3+}$	13.6	1.542
+2		
$\mathbf{2o}^{2+}$ (antipar)	0	3.583
TS	190.1	1.728
$\mathbf{2c}^{2+}$	74.9	1.532
+1		
$\mathbf{2o}^{+}$ (antipar)	0	3.528
TS	89.1	2.082
$\mathbf{2c}^{+}$	−8.0	1.537
0		
2o (antipar)	0	3.280
TS	16.3	2.460
2c	−120.8	1.546

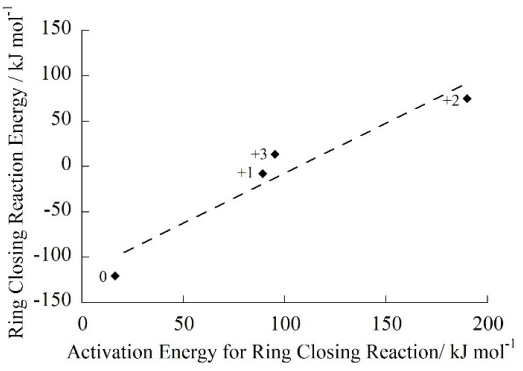

Figure 8. Correlation between the activation energy of the ring-closure and the energy difference in the ground state between the open and closed forms for each of the redox states of the switch **2**.

Ground state reactivity: ring-opening reaction

The activation energy (E_a) of the closed form for each of the four redox states has been computed and compared with the experimentally available one for the dicationic state (Table 4).

In addition to the good agreement between the calculated and experimental value of E_a in the dicationic state **2c**$^{2+}$, calculated data also reveal a strong impact of the redox state on the activation energy of the ground state ring-opening reaction. Clearly, oxidation of **2c**$^{2+}$ destabilizes the closed form and makes the ring-opening reaction easier, with a smaller E_a (81.6 kJ.mol^{-1}).

Electronic properties: redox properties

From the photoactive open form (**2o**$^{n+}$) and closed form (**2c**$^{n+}$), i.e. the antiparallel open form and the resulting closed ones, the redox potentials were calculated in acetonitrile according to the thermodynamic cycle shown in Scheme 4 (Scheme S2 in the Supporting Information for details). Results are gathered in Table 5 and compared with the experimental ones.

The calculated results for the open form are in fully agreement with the experimental ones measured by cyclic voltammetry. The reduction of **2o**$^{2+}$ at −0.91 V is a one-electron process on each of the two electronically quite de-coupled N-methyl pyridinium groups. Concerning the closed form, the only observed redox couple at −0.21 V (vs. SCE) probably results from two close one-electron redox couples which, under the experimental conditions, remain unresolved.

Table 4. Calculated ring-opening activation energy vs. experimental one

Redox state	**2c**$^{3+}$	**2c**$^{2+}$	**2c**$^{+}$	**2c**
E_a (kJ/mol) calc.	81.6	115.3	97.1	137.0
E_a (kJ/mol) exp.		94		

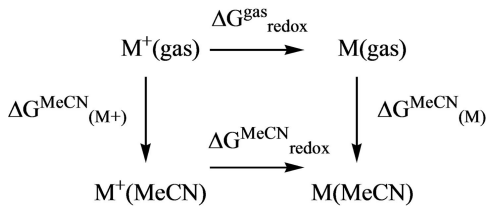

Scheme 4. Thermodynamic cycle for the computation of redox properties.

Table 5. Computed redox potentials vs. experimental ones of the switch **2**.

	Calc. E (V vs. SCE)		Exp. E (V vs. SCE)
2o^{2+} to **2o**$^{+}$	−1.00	**2o**$^{2+}$ to **2o**	−0.91
2o^{+} to **2o**	−1.78		
2c^{2+} to **2c**$^{+}$	−0.26	**2c**$^{2+}$ to **2c**	−0.21
2c^{+} to **2c**	−0.58		
2c^{2+} to **2c**$^{3+}$	0.85	**2c**$^{2+}$ to **2c**$^{3+}$	1.10

Electronic properties: optical properties

TD-DFT calculations were used to identify the nature of the electronic absorptions associated with the dicationic and neutral redox state of open and closed form of the switch **2**.

The calculated vertical electronic transition of the open and closed forms of the switch in its dicationic and neutral states are listed in Table 6 and compared with the experimental values. The calculated spectra are presented in Figure 9.

The UV/vis spectrum of **2o**$^{2+}$ is dominated by two electronic transitions (λ_{exp}: 375 and 322 nm). The calculations give quite accurate results with three electronic transitions where two of them are very close and can give overlapping of the absorption bands. The calculations underestimate the wavelengths with an error of 20 nm (λ_{calc}: 353 and 301 nm). The absorption spectrum of the closed form **2c**$^{2+}$ is dominated in the 300–700 nm region by three electronic transitions (λ_{exp}: 744, 430 and 277 with a shoulder centered at 320 nm). The calculations give very good results for the lower energy band (λ_{calc}: 739 nm) but overestimate the results for higher energies. The error is of 24 nm for the visible band (λ_{calc}: 454 nm instead of λ_{exp}: 430 nm) and of 100 nm for the UV band (λ_{calc}: 373 nm instead of λ_{exp}: 277 nm).

The UV/Vis of the two-electron reduced open form **2o** is characterized by one very intense electronic absorption in the

Table 6. Computed energies of vertical electronic transition of the dicationic and neutral forms of the switch **2**. Only the wavelengths and oscillator strengths of relevant transitions are listed and compared with experimental values.

	λ_{calc} (nm)	λ_{exp} (nm)	f	Assignment
2o^{2+}	353	375	0.789	HOMO to LUMO
	300	322	0.681	HOMO to LUMO+2
	250		0.421	HOMO-1 to LUMO+1
2c^{2+}	740	744	0.538	HOMO to LUMO
	454	430	0.305	MOMO to LUMO+1
	373	277 (320 sh)	0.362	HOMO-1 to LUMO
2o	407	420	0.393	HOMO to LUMO+6
2c	635	725	1.431	HOMO to LUMO
	494	535	0.311	HOMO-1 to LUMO
	420	289	0.361	HOMO to LUMO+1

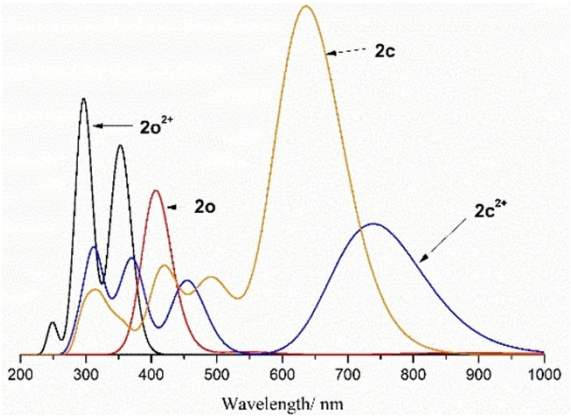

Figure 9. Calculated electronic spectra of **2o**$^{2+}$, **2c**$^{2+}$, **2o** and **2c**.

visible range (λ_{exp}: 420 nm) and the calculations also give one electronic transition with a small underestimated value of the energy band (λ_{calc}: 407 nm). Concerning the two-electron reduced closed form **2c**, the two electronic absorptions in the visible range (λ_{exp}: 725 nm and λ_{exp}: 535 nm) are reproduced by calculations but with a large error, particularly for the lower energy band (λ_{calc}: 635 nm and λ_{calc}: 492 nm). Nevertheless, the blue-shift and the enhancement in intensity of the lower energy band by reduction are reproduced by the calculations.

The main frontier orbitals of $\mathbf{2o}^{2+}$, $\mathbf{2c}^{2+}$, **2o** and **2c** are reported in the Supporting Information (Figure S7). The most interesting results are the difference of the orbitals involved in the visible absorption of the closed form. For the dicationic redox state $\mathbf{2c}^{2+}$ the maximum absorption at 740 nm is issued from the HOMO→LUMO transition which involves orbitals localized on the hexatriene core of the molecule as well as the lateral conjugated arms. The absorption at 454 nm of the same redox state involves the HOMO→LUMO+1 transition, localized on the same part of the molecule. In the case of the neutral closed form **2c** the maximum absorption at 635 nm and the two weak visible absorptions at 494 and 420 nm are based on HOMO-1, HOMO to LUMO, LUMO+1 transitions which involve, like the dicationic form, orbitals localized on the hexatriene part of the molecule as well as the lateral conjugated arms, but also orbitals (LUMO and LUMO+1) built with large contribution of the central conjugated bridge.

Finally, we attempted to simulate the evolution of the UV-Vis spectra recorded during the electrolysis (Figure 5a and b) by adding different weight of the just described species. Concerning the reduction at −1.10 V we assumed the sequential mechanism $\mathbf{2o}^{2+}$→**2o** and then **2o**→**2c**, with the total reduction of $\mathbf{2o}^{2+}$ to **2o** followed by full conversion of **2o** into **2c**. For each step, the change of the spectra is taking into account the weighted sums of the different spectra of initial and final state of the two sequences from initial and final states of the two sequences. The evolution is shown in Figure 10 and is in agreement with the experimental one presented in Figure 5a (reduction of the open form $\mathbf{2o}^{2+}$ at −1.10 V). We first noticed the occurrence of an absorption band at 407 nm, compatible with the formation of **2o**, while the band at 250 and 353 nm assigned to the dicationic open form $\mathbf{2o}^{2+}$ disappears. Then, the band at 407 nm fades away in favor of two new absorption bands at 494 and 635 nm, which are correlated to the experimental ones at 535 and 725 nm. The nice agreement between the simulated and experimental data strongly supports the cyclization pathway through the two-electron reduced open form **2o**.

Simulation of the second step of the electrolysis at 0.0 V was also considered. Given the experimental data (Figure 5b), only one step mechanism **2c**→$\mathbf{2c}^{2+}$ is considered. The calculated spectral evolution of **2c** to $\mathbf{2c}^{2+}$ is shown in Figure 11. As previously mentioned, we attributed the calculated absorption bands at 494 nm and 635 nm to the experimental ones at 725 and 535 nm. The calculated evolution of **2c** to $\mathbf{2c}^{2+}$ shows the redshift of the band at 635 nm in favor of the less intense at 740 nm. At the same time the absorption band at 494 nm vanishes and a new one appears at 454 nm.

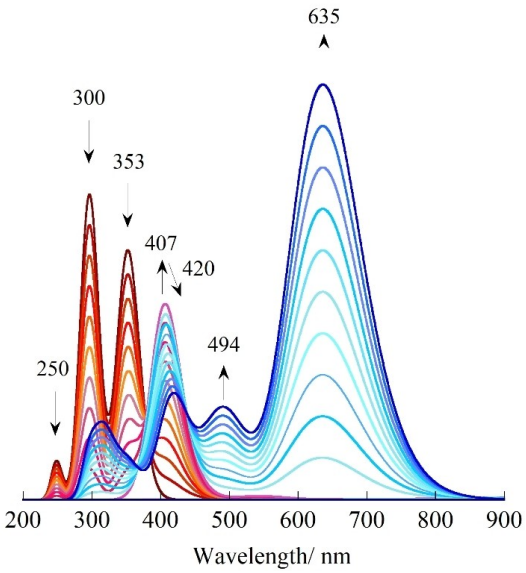

Figure 10. Calculated absorption spectral evolution of the reduction of $\mathbf{2o}^{2+}$ to the neutral **2o** and then the spontaneous ring-closure to the neutral **2c**.

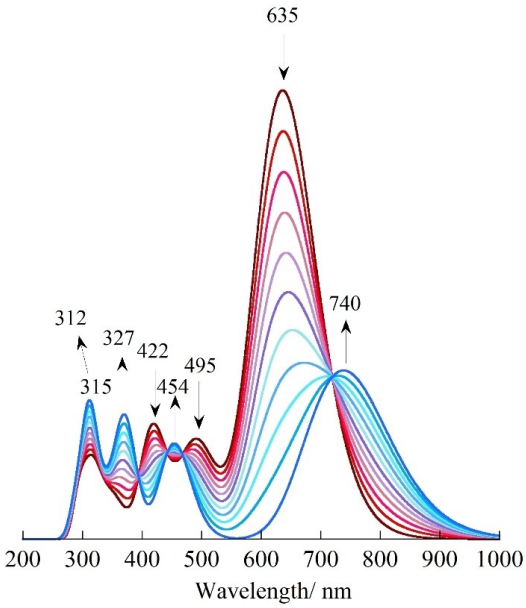

Figure 11. Calculated absorption spectral evolution of the oxidation of the neutral **2c** to the dicationic $\mathbf{2c}^{2+}$.

Those two absorption bands at 740 nm and 454 nm were previously attributed to the experimental bands of the dicationic closed form $\mathbf{2c}^{2+}$ (respectively 744 and 430 nm). We are also able to correlate the decrease of the calculated absorption band at 422 nm in agreement with experimental one at 404 nm and the increase of the calculated absorption bands at 367 and 454 nm in agreement with the 330 and 431 experimental bands. Finally, the small blue-shift from 315 nm to 312 nm and the increase in intensity of the calculated band can

be attributed to the shift and evolution of the experimental band from 293 nm to 277 nm.

Concerning the ferrocene substituted dicationic switch $\mathbf{4}^{2+}$, a very similar correlation is found between its oxidation state and the ground state stability except for the triple positively charged state where the closed form $\mathbf{4c}^{3+}$ is much more destabilized compared to $\mathbf{4o}^{3+}$ than $\mathbf{2c}^{3+}$ versus $\mathbf{2o}^{3+}$ (Table S2), and this is in line with the observed acceleration of the thermal ring-opening when $\mathbf{4c}^{2+}$ is oxidized to $\mathbf{4c}^{3+}$ (Figure 4b). Moreover, TD-DFT calculations also reveal that the low energy and low intensity bands of $\mathbf{4o}^{2+}$ (Figure S8) are made up of pure ferrocene-based transitions and also some transitions which, because of their charge transfer characters, may account, at least in part, for its low photochemical reactivity.

Conclusion

In summary, a terthiazolylene capable of bi-directional photo- and redox-switching, the first among terarylenes, is synthesized and fully characterized. For the redox-switching, the presence of the two lateral N-methyl pyridinium groups in the structure of the terthiazole is crucial not only to the ring-closure at a readily accessible reduction potential but also, in a rather counterintuitive way, to the oxidative ring-opening reaction. The reductive ring-closure is found to be a bi-electronic process and proceeds via the two-electron reduced open form. As revealed by the DFT calculations, the driving force for both the reductive ring-closure and the oxidative ring-opening is the energy difference in the ground state between the open and closed forms, and this difference is strongly impacted by the oxidation state of the switch, highlighting the fundamental difference and also the complementarity between the two switching modes. Introduction of a ferrocene substituent on the central thiazolyl moiety is found to be detrimental to the photochromism of the switch but not to its redox switchability. Instead, its presence allows to speed up the ring-opening reaction at a much lower potential via the oxidation of ferrocene to ferrocenium. Finally, it is worth noting another appealing feature of such a photo- and redox-switch: the large difference in the redox potential between its open and closed forms (700 mV) means that a part of the photon energy necessary to trigger the cyclization is stored in the form of chemical potential available for other works. For instance, the switch in its open form can be viewed as a hidden electron acceptor that is stronger than the well-known methyl viologen[37] and photo-activable at will.

Experimental section

Detailed descriptions of experimental methods, synthetic procedures, characterizations of new compounds, X-Ray analysis (CCDC 2084834) as well as additional spectroscopic and calculation data can be found in the Supporting Information.

Acknowledgements

The Agence Nationale de la Recherche is gratefully acknowledged for the support (ANR-17-CE07-0056).

Conflict of Interest

The authors declare no conflict of interest.

Keywords: density functional calculations · photochromism · photoswitches · redoxswitches · terarylenes

[1] Some recent reviews: a) W. Danowski, T. van Leeuwen, W. R. Browne, B. L. Feringa, *Nanoscale Adv.* **2021**, *3*, 24–40; b) A. Goulet-Hanssens, F. Eisenreich, S. Hecht, *Adv. Mater.* **2020**, *32*, 1905966; c) I. M. Welleman, M. W. H. Hoorens, B. L. Feringa, H. H. Boersma, W. Szymanski, *Chem. Sci.* **2020**, *11*, 11672–11691; d) X. Huang, T. Li, *J. Mater. Chem. C* **2020**, *8*, 821–848; e) M. Jeong, J. Park, S. Kwon, *Eur. J. Org. Chem.* **2020**, 7254–7283; f) S. P. Ihrig, F. Eisenreich, S. Hecht, *Chem. Commun.* **2019**, *55*, 4290–4298; g) Z. L. Pianowski, *Chem. Eur. J.* **2019**, *25*, 5128–5144; h) L. Wang, Q. Li, *Chem. Soc. Rev.* **2018**, *47*, 1044–1097; i) X. Zhang, L. Hou, P. Samori, *Nat. Commun.* **2016**, *7*, 11118; j) M. M. Lerch, M. J. Hansen, G. M. van Dam, W. Szymanski, B. L. Feringa, *Angew. Chem. Int. Ed.* **2016**, *55*, 10978–10999; *Angew. Chem.* **2016**, *128*, 11140–11163.

[2] a) M. Irie, *Chem. Rev.* **2000**, *100*, 1685–1716; b) M. Irie, T. Fukaminato, K. Matsuda, S. Kobatake, *Chem. Rev.* **2014**, *114*, 12174–12277.

[3] T. Koshido, T. Kawai, K. Yoshino, *J. Phys. Chem.* **1995**, *99*, 6110–6114.

[4] a) A. Peters, N. R. Branda, *Chem. Commun.* **2003**, 954–955; b) A. Peters, N. R. Branda, *J. Am. Chem. Soc.* **2003**, *125*, 3404–3405.

[5] Y. Moriyama, K. Matsuda, N. Tanifuji, S. Irie, M. Irie, *Org. Lett.* **2005**, *7*, 3315–3318.

[6] a) W. R. Browne, J. J. D. de Jong, T. Kudernac, M. Walko, L. N. Lucas, K. Uchida, J. H. van Esch, B. L. Feringa, *Chem. Eur. J.* **2005**, *11*, 6414–6429; b) W. R. Browne, J. J. D. de Jong, T. Kudernac, M. Walko, L. N. Lucas, K. Uchida, J. H. van Esch, B. L. Feringa, *Chem. Eur. J.* **2005**, *11*, 6430–6441.

[7] G. Guirado, C. Coudret, M. Hliwa, J. P. Launay, *J. Phys. Chem. B* **2005**, *109*, 17445–17459.

[8] G. Guirado, C. Coudret, J. P. Launay, *J. Phys. Chem. C* **2007**, *111*, 2770–2776.

[9] J. Areephong, W. R. Browne, N. Katsonis, B. L. Feringa, *Chem. Commun.* **2006**, 3930–3932.

[10] H. Logtenberg, J. H. M. van der Velde, P. de Mendoza, J. Areephong, J. Hjelm, B. L. Feringa, W. R. Browne, *J. Phys. Chem. C* **2012**, *116*, 24136–24142.

[11] M. Kleinwächter, E. Teichmann, L. Grubert, M. Herder, S. Hecht, *Beilstein J. Org. Chem.* **2018**, *14*, 2812–2821.

[12] B. Gorodetsky, H. D. Samachetty, R. L. Donkers, M. S. Workentin, N. R. Branda, *Angew. Chem. Int. Ed.* **2004**, *43*, 2812–2815; *Angew. Chem.* **2004**, *116*, 2872–2875.

[13] B. Gorodetsky, N. R. Branda, *Adv. Funct. Mater.* **2007**, *17*, 786–796.

[14] A. Léaustic, E. Anxolabéhère-Mallart, F. Maurel, S. Midelton, R. Guillot, R. Métivier, K. Nakatani, P. Yu, *Chem. Eur. J.* **2011**, *17*, 2246–2255.

[15] I. Gallardo, G. Guirado, M. Moreno, G. Prats, M. Takeshita, *Chem. Eur. J.* **2012**, *18*, 9807–9812.

[16] T. Nakashima, K. Atsumi, S. Kawai, T. Nakagawa, Y. Hasegawa, T. Kawai, *Eur. J. Org. Chem.* **2007**, 3212–3218.

[17] S. Kawai, T. Nakashima, Y. Kutsunugi, H. Nakagawa, H. Nakano, T. Kawai, *J. Mater. Chem.* **2009**, *19*, 3606–2611.

[18] F. Fukumoto, T. Nakashima, T. Kawai, *Angew. Chem. Int. Ed.* **2011**, *50*, 1565–1568; *Angew. Chem.* **2011**, *123*, 1603–1606.

[19] S. Chen, Y. Yang, Y. Wu, H. Tian, W. Zhu, *J. Mater. Chem.* **2012**, *22*, 5486–5494.

[20] P. H.-M. Lee, C.-C. Ko, N. Zhu, V. W.-W. Yam, *J. Am. Chem. Soc.* **2007**, *129*, 6058–6059.

[21] C.-T. Poon, W. H. Lam, H.-L. Wong, V. W.-W. Yam, *J. Am. Chem. Soc.* **2010**, *132*, 13992–13993.

[22] Z. Xu, Q. T. Liu, X. Wang, Q. Liu, D. Hean, K. C. Chou, M. O. Wolf, *Chem. Sci.* **2020**, *11*, 2729–2734.

[23] J. Guérin, A. Léaustic, J. Berthet, R. Métivier, R. Guillot, S. Delbaere, K. Nakatani, P. Yu, *Chem. Asian J.* **2017**, *12*, 853–859.
[24] T. Nakashima, Y. Kajiki, S. Fukumoto, M. Taguchi, S. Nagao, S. Hirota, T. Kawai, *J. Am. Chem. Soc.* **2012**, *134*, 19877–19883.
[25] J. P. Calupitan, T. Nakashima, Y. Hashimoto, T. Kawai, *Chem. Eur. J.* **2016**, *22*, 10002–10008.
[26] K. Uchida, T. Ishikawa, M. Takeshita, M. Irie, *Tetrahedron* **1998**, *54*, 6627–6638.
[27] S. Takami, T. Kawai, M. Irie, *Eur. J. Org. Chem.* **2002**, 3796–3800.
[28] M. Giraud, A. Léaustic, M.-F. Charlot, P. Yu, M. Césario, C. Philouze, R. Pansu, K. Nakatani, E. Ishow, *New J. Chem.* **2005**, *29*, 439–446.
[29] S. Kawai, T. Nakashima, K. Atsumi, T. Sakai, M. Harigai, Y. Imamoto, H. Kamikubo, T. Kawai, *Chem. Mater.* **2007**, *19*, 3479–3483.
[30] Y. Wu, Y. Xie, Q. Zhang, H. Tian, W. Zhu, A. D. Q. Li, *Angew. Chem. Int. Ed.* **2014**, *53*, 2090–2094; *Angew. Chem.* **2014**, *126*, 2122–2126.
[31] Y. Cai, Y. Gao, Q. Luo, M. Li, J. Zhang, H. Tian, W. Zhu, *Adv. Opt. Mater.* **2016**, *4*, 1410–1416.
[32] S. Kobatake, K. Uchida, E. Tsuchida, M. Irie, *Chem. Commun.* **2002**, 2804–2805.
[33] M. Herder, M. Utecht, N. Manicke, L. Grubert, M. Pätzel, P. Saalfranck, S. Hecht, *Chem. Sci.* **2013**, *4*, 1028–1040.
[34] R. Kanazawa, T. Nakashima, T. Kawai, *J. Phys. Chem. A* **2017**, *121*, 1638–1646.
[35] J. M. Park, C. Y. Jung, W.-D. Jang, J. Y. Jaung, *Dyes Pigm.* **2020**, *177*, 108315.
[36] M. G. Evans, M. Polanyi, *J. Chem. Soc. Faraday Trans.* **1936**, *32*, 1333–1360.
[37] K. Takahashi, *Pure Appl. Chem.* **1993**, *65*, 127–134.

Manuscript received: June 2, 2021
Accepted manuscript online: July 2, 2021
Version of record online: ■■, ■■■

FULL PAPER

Molecular switches are key elements for the design of stimuli-responsive systems and materials. Of particular interest are switches that can be fully operated both by light and electricity, the two most popular inputs. It is shown for the first time that a terarylene photoswitch can be effectively transformed to an efficient photo and redox one when decorated with the electroactive N-methyl pyridinium group. The driving forces behind different switching processes are revealed by a joint experimental and theoretical approach.

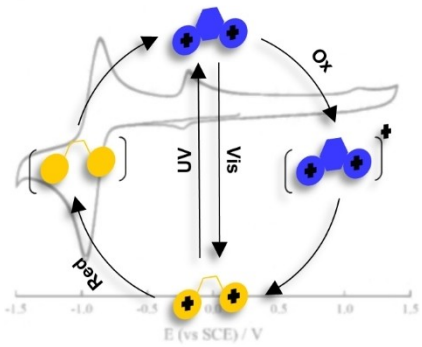

N. Baggi, Dr. A. Léaustic, Dr. S. Groni, Dr. E. Anxolabéhère-Mallart, Dr. R. Guillot, Dr. R. Métivier, Prof. F. Maurel*, Dr. P. Yu**